

Photon-photon polaritons in $\chi^{(2)}$ microresonators

D.V. Skryabin,^{1,2,*} V.V. Pankratov,¹ A. Villois,¹ and D.N. Puzyrev¹

¹*Department of Physics, University of Bath, Bath, BA2 7AY, UK*

²*Russian Quantum Centre, Skolkovo 121205, Russia*

(Dated: Submitted 20 July 2020, revised 02 November 2020)

We consider a high-Q microresonator with $\chi^{(2)}$ nonlinearity under conditions when the coupling rates between the sidebands around the pump and second harmonic exceed the damping rates, implying the strong coupling regime (SC). Using the dressed-resonator approach we demonstrate that this regime leads to the dominance of the Hermitian part of the operator driving the side-band dynamics over its non-Hermitian part responsible for the parametric gain. This has allowed us to introduce and apply the cross-area concept of the polariton quasi-particles and define their effective masses in the context of $\chi^{(2)}$ ring-microresonators. We further use polaritons to predict the modified spectral response of the resonator to a weak probe field, and to reveal splitting of the bare-resonator resonances, avoided crossings, and Rabi dynamics. Polariton basis also allows deriving a discrete sequence of the parametric thresholds for the generation of sidebands of different orders.

I. INTRODUCTION

Strong coupling (SC) between photons and matter is at the heart of modern cavity quantum electrodynamics [1]. Some of the currently burgeoning areas underpinned by the SC physics are quantum communication [2], microresonator exciton-polaritons [3–9], artificial fields, atoms, and dimensions, and topological effects [10–12].

A common SC setup involves a mode of the high-finesse resonator interacting with a transition between the material energy levels. If the coupling rate is large relative to the dissipation rates, then the system can sustain multiple oscillations between the light and matter states [13–15]. The prime parameter behind properties of these oscillations is Rabi frequency, Ω . SC regime is most suitably described by the dressed eigenstates hybridising the light and matter degrees of freedom [16–19]. If the energy-momentum relation, $\varepsilon(k)$, is introduced for the dressed states, then one can also define quasi-particles or elementary excitations [20]. A list of hybrid light-matter quasi-particles, or polaritons, includes exciton-polaritons [3–7], plasmon-polaritons [21, 22], EIT-polaritons (electromagnetically induced transparency) [23], etc. Polaritons are not only a powerful theoretical concept, but are also a striking experimental feature associated with splitting and avoided crossing of the energy levels, and with Bose-Einstein condensation, see, e.g., [3–5, 22].

While chip-integrated and bulk-cut high-Q ring microresonators continue to push limits of frequency comb research [24, 25], some experimental results are also pointing towards potential these devices hold to study SC. E.g., Ref. [26] reported SC between the whispering gallery modes and atoms, Ref. [27] studied the EIT-like regimes in two coupled resonators, and Ref. [28] described measurements of the low-contrast resonance splitting effects using non-degenerate $\chi^{(3)}$ four-wave mixing

(FWM). Refs. [29, 30] developed theories for SC between two sidebands in $\chi^{(3)}$ FWM without exploring the possibility to introduce the energy-momentum relations and quasi-particles.

Monolithic- and microresonator devices with $\chi^{(2)}$ nonlinearity have been a viable and long-existing option complementing the mainstream of $\chi^{(3)}$ work, see, e.g. [31–37]. Ref. [38] considered SC between the pump and single-mode 2nd harmonic photons in a planar semiconductor cavity. $\chi^{(2)}$ response generally provides larger nonlinear phase shifts than $\chi^{(3)}$ [33], which is a factor increasing the coupling between sidebands. This is also complemented by the recent progress with simultaneous reduction of losses and volumes of $\chi^{(2)}$ microresonators [39–44]. A combination of these factors favours considering if a multimode $\chi^{(2)}$ microresonator could go beyond simply modifying the light-matter interaction by reducing the density of states, i.e., Purcell regime, available for photon transitions and to cross into the SC regime, where new families of states (dressed states, and associated energy levels) are created.

Below, we demonstrate that $\chi^{(2)}$ microresonators with Q approaching 10^8 [33–37], can operate in the SC regime between the sidebands centred around the pump (ordinary polarised) and second harmonic (extraordinary) frequencies. The SC regime becomes accessible far from the resonance, well outside the bistability and soliton regimes [43]. We parametrise energies of the dressed, i.e., hybrid ordinary-extraordinary, states with their momenta, and define microresonator quasi-particles - *photon-photon polaritons*. They are different from the above-mentioned families of the exciton-polaritons in planar [3–9] and ring [45] semiconductor microresonators, and from other polaritons involving transitions between the real, e.g. molecular [46], levels, because they do not require such absorbing transitions to exist in the matter component of the hybrid states. Instead, the matter side of the photon-photon polaritons belongs to the continuum of virtual, i.e., far-away from resonances, electronic transitions. $\chi^{(2)}$ nonlinearity induced by these transitions is broad-band, and practically non-absorbing and non-dispersive.

* d.v.skryabin@bath.ac.uk

II. MODEL

The envelopes of the ordinary, ψ_o (fundamental), and of the extraordinary, ψ_e (2nd harmonic), fields in a microresonator are expressed via their mode expansions as $\psi_s = \sum_{\mu} \psi_{\mu s}(t) e^{i\mu\vartheta}$, with $s = o, e$ been the polarization state index. $\vartheta \in [0, 2\pi)$ is the polar angle varying along the resonator circumference, and $\mu = 0, \pm 1, \pm 2, \dots$ are the relative mode numbers, i.e., momenta. The associate resonance frequencies are $\omega_{\mu s} = \omega_{0s} + \mu D_{1s} + \frac{1}{2}\mu^2 D_{2s}$, where $D_{1s}/2\pi$ are the repetition rates (free spectral ranges, FSRs) and D_{2s} are the dispersions. Detunings of the resonator frequencies $\omega_{\mu o}$ and $\omega_{\mu e}$ from the pump laser frequency, ω_p , and $2\omega_p$ are $\delta_{\mu o} = \omega_{\mu o} - \omega_p$ and $\delta_{\mu e} = \omega_{\mu e} - 2\omega_p$, respectively.

Equations driving the envelope dynamics are [47]

$$\begin{aligned} i\partial_t \psi_o &= \delta_o \psi_o - iD_{1o} \partial_{\vartheta} \psi_o - \frac{1}{2} D_{2o} \partial_{\vartheta}^2 \psi_o \\ &\quad - \gamma_o \psi_e \psi_o^* - i\frac{1}{2} \kappa_o (\psi_o - \mathcal{H}), \\ i\partial_t \psi_e &= \delta_e \psi_e - iD_{1e} \partial_{\vartheta} \psi_e - \frac{1}{2} D_{2e} \partial_{\vartheta}^2 \psi_e \\ &\quad - \gamma_e \psi_o^2 - i\frac{1}{2} \kappa_e \psi_e. \end{aligned} \quad (1)$$

Here $\delta_o \equiv \delta_{0o}$, and $\delta_e \equiv \delta_{0e} = 2\delta_o - (2\omega_{0o} - \omega_{0e})$. $\mathcal{H}^2 = \eta \mathcal{F} \mathcal{W} / \pi$ is the intra-resonator pump power, \mathcal{W} is the 'on-chip' laser power, $\mathcal{F} = D_{1o} / \kappa_o \sim 10^4$ is finesse, and $\eta < 1$ is the coupling efficiency. κ_s are the loaded linewidth parameters. γ_s are the nonlinear coefficients measured in $\text{Hz}/\text{W}^{1/2}$ [47], see also [48] for more details. A Galilean transformation to the reference frame rotating with the rate $D_1/2\pi$, $\theta = \vartheta - D_1 t$, converts detunings to

$$\Delta_{\mu s} = \delta_{\mu s} - \mu D_1. \quad (2)$$

III. DRESSED-RESONATOR METHOD

CW-solution of Eqs. (1), $\partial_{\theta} \tilde{\psi}_s = \partial_t \tilde{\psi}_s = 0$, is sought in the form $\tilde{\psi}_o / \mathcal{H}_* = \Omega / \Omega_*$, where $\Omega_* = \sqrt{2\kappa_o \kappa_e} \simeq 2\pi \times 6.3 \text{MHz}$ is the characteristic frequency scale defined by the linewidths, and $\mathcal{H}_*^2 = \kappa_o \kappa_e / 4\gamma_{2o} \gamma_{2e} \simeq 55 \mu\text{W}$ is the intra-resonator power scale. Thus, Ω is the frequency measure of the intra-resonator field, and, as we will see below, it has meaning of the Rabi frequency.

CW-state power is now expressed via modulus of Ω , $|\tilde{\psi}_o|^2 = \mathcal{H}_*^2 |\Omega|^2 / \Omega_*^2$, and straightforward algebra with Eqs. (1) reveals that Ω is a solution of

$$i \frac{\Omega}{\Omega_*} \cdot \frac{\Omega_o}{\kappa_o/2} \left(1 - \frac{|\Omega|^2}{\Omega_o \Omega_e} \right) = \frac{\mathcal{H}}{\mathcal{H}_*} = \sqrt{\frac{\mathcal{W}}{\mathcal{W}_*}}, \quad (3)$$

and that the 2nd harmonic amplitude is $\tilde{\psi}_e = \Omega^2 / \Omega_e \gamma_o$. Here $\mathcal{W}_* = \pi \mathcal{H}_*^2 / \eta \mathcal{F} \simeq 16 \text{nW}$ is the 'on-chip' pump power scale, and $\Omega_o \equiv (\delta_o - i\kappa_o/2)$, $\Omega_e \equiv 8(\delta_e - i\kappa_e/2)$ are the complex frequencies introduced for the sake of brevity.

Following the ethos of the dressed-atom theory [16–19], we apply the dressed-resonator method consisting

from (i) expanding the small amplitude perturbations around the cw-state using the modes of the linear resonator, (ii) separating the Hermitian and non-Hermitian parts of the operator driving the evolution of the perturbations, and (iii) identifying the eigenstates of the Hermitian part, i.e., dressed-states or polaritons.

We now look for a solution of Eqs. (1) in the form, $\psi_s = \tilde{\psi}_s + q_s e^{i\phi_s} \sum_{\mu} (a_{\mu s}(t) e^{i\mu\theta} + a_{-\mu s}^*(t) e^{-i\mu\theta})$, where $q_o = 1/\sqrt{2}$, $q_e = \sqrt{\gamma_e/\gamma_o}$ and $\phi_s = \arg \tilde{\psi}_s$. Assuming that the sideband amplitudes, $|a_{\mu s}|$, are small we find

$$i\partial_t |a_{\mu}\rangle = (\hat{H}_{\mu} + \hat{V}) |a_{\mu}\rangle. \quad (4)$$

Here $|a_{\mu}\rangle = (a_{\mu o}, a_{\mu e}, a_{-\mu o}, a_{-\mu e})^T$ is the state vector,

$$\hat{H}_{\mu} = \begin{bmatrix} \Delta_{\mu o} & -\frac{1}{2} |\Omega| e^{-i\phi} & 0 & 0 \\ -\frac{1}{2} |\Omega| e^{i\phi} & \Delta_{\mu e} & 0 & 0 \\ 0 & 0 & -\Delta_{-\mu o} & \frac{1}{2} |\Omega| e^{i\phi} \\ 0 & 0 & \frac{1}{2} |\Omega| e^{-i\phi} & -\Delta_{-\mu e} \end{bmatrix}, \quad (5)$$

$\phi = 2\phi_o - \phi_e$, and

$$\hat{V} = \begin{bmatrix} -i\frac{1}{2} \kappa_o & 0 & -\frac{|\Omega|^2}{|\Omega_e|} e^{-i\phi} & 0 \\ 0 & -i\frac{1}{2} \kappa_e & 0 & 0 \\ \frac{|\Omega|^2}{|\Omega_e|} e^{i\phi} & 0 & -i\frac{1}{2} \kappa_o & 0 \\ 0 & 0 & 0 & -i\frac{1}{2} \kappa_e \end{bmatrix}, \quad (6)$$

The diagonal terms in \hat{H}_{μ} make up the Hamiltonian of the bare, i.e., undressed, resonator. $\Omega \neq 0$ provides dressing and, importantly, retains the Hermitian structure. The diagonal terms in \hat{H}_{μ} are $\sim |\Omega|^1$, and drive the flopping between the bare ordinary and extraordinary states with the same μ , see the state-vector structure. Therefore, Ω has the meaning of the Rabi frequency. Like in the two-level atom case [18, 19], the bare states are separated by the optical frequency, i.e., by the energy $\sim eV$. While, the level splitting is characterised by the radio-frequency (RF) scale, $\hbar|\Omega| \lesssim 1 \mu\text{eV}$ [48]. The off-diagonal terms in \hat{H}_{μ} are the three-wave mixing (TWM) ones, since they describe adding one $\mu = 0$ ordinary photon, defined by the $|\Omega|^1$ -term, $\Omega \sim \tilde{\psi}_o$, to one ordinary $\mu \neq 0$ photon to generate one extraordinary photon with the same μ . The two-level atom methodology was also previously developed for the resonator-free sum-frequency generation, see, e.g., [49, 50].

Interaction between the μ and $-\mu$ ordinary photons is governed by the off-diagonal terms in \hat{V} . These are the four-wave mixing (FWM) terms engaging two $\mu = 0$ ordinary photons, coming from $|\Omega|^2$, and two side-band ones, which are also ordinary, but have momenta $\pm\mu$. For studies into the FWM gain in $\chi^{(2)}$ materials see, e.g., Refs. [33, 51]. \hat{V} also includes dissipation, that competes with the FWM gain. Therefore, the sideband dynamics is expected to be dominated by the TWM Rabi dynamics for $\|\hat{H}_{\mu}\| \gg \|\hat{V}\|$. This constitutes the SC conditions, which can be expressed as $|\Omega_e| \gg |\Omega| \gg \Omega_*$.

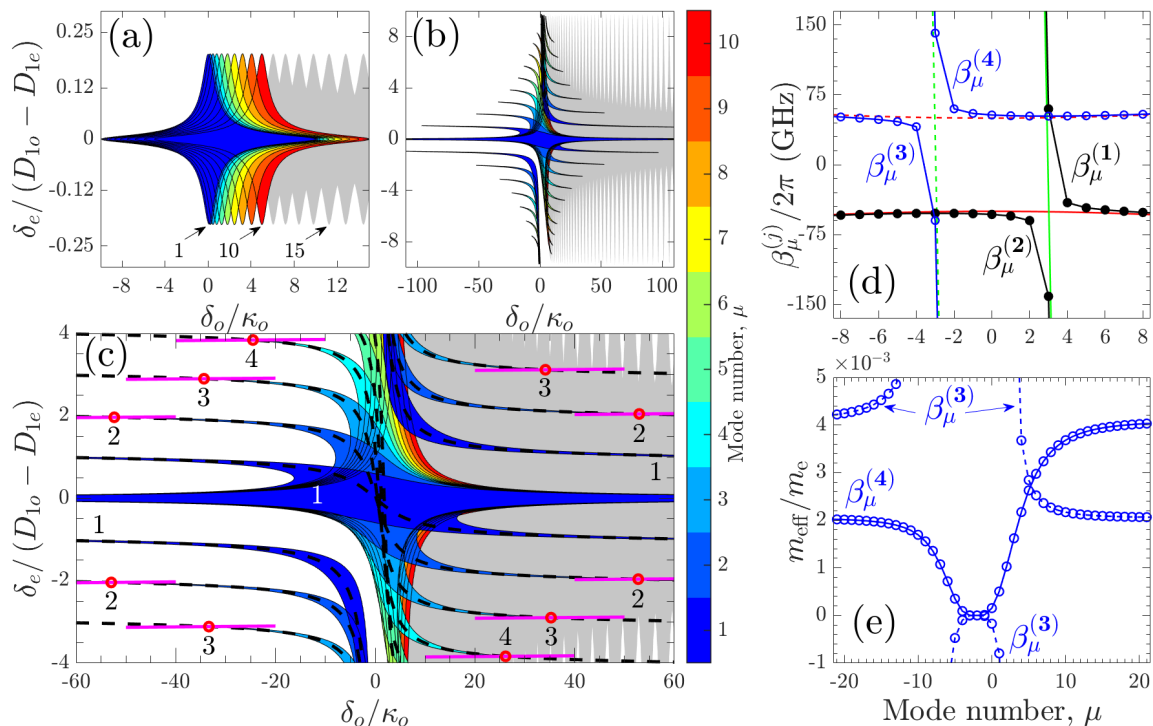


FIG. 1. **(a-b)** Reshaping of the $\mu \neq 0$ parametric instability boundaries for $|\Omega|$ increasing from $28 \times \kappa_o$ (a) to $200 \times \kappa_o$ (b). Coloured and grey shading cover the unstable domains. **(c)** shows the finer details of (b). Red points mark the tips of the unstable tongues, and the numbers are the respective μ 's. Dashed black lines show the resonance condition, Eq. (10), and the short magenta lines show the threshold conditions $V_\mu^{(j_1 j_2)} V_\mu^{(j_2 j_1)} = V_\mu^{(j_1 j_1)} V_\mu^{(j_2 j_2)}$; $j_1, j_2 = 2, 4$ in the 1st quadrant; 1, 4 in the 2nd and 4th; 1, 3 in the 3rd. Other parameters are $(D_{1o} - D_{1e})/\kappa_o = 10^3$, $D_{2o}/\kappa_o = -0.1$, $D_{2e}/\kappa_o = -0.2$. The colorbar shows the correspondence between the colors and the mode-numbers, $|\mu|$. **(d)** The photon-photon frequency $\beta_\mu^{(j)}$ vs momentum μ : $\delta_o/\kappa_o = -50$, $\delta_e/(D_{1o} - D_{1e}) = 2.97$, are taken close to the $\mu = 3$ tip in (c). Red and green lines without circles mark the bare, $\Omega = 0$, spectrum of \hat{H}_μ . The avoided crossings are centred at $\Delta_\mu = 0$ and $\Delta_{-\mu} = 0$. **(e)** Effective photon-photon mass, m_{eff} , relative to the electron mass, m_e , for the $\beta_\mu^{(3)}$ (dashed line), and $\beta_\mu^{(4)}$ (full line) branches from (d).

$|\Omega| \gg \Omega_* \equiv \sqrt{2\kappa_o \kappa_e}$ is achieved by taking a high-Q resonator and the relatively strong pump, while $|\Omega| \ll |\Omega_e|$ implies small conversion efficiency to the 2nd harmonic due to large value of the frequency mismatch parameter, $|2\omega_{0o} - \omega_{0e}| \sim |\Omega_e|/8$. Note, that Eq. (3) can be linearised for $|\Omega|^2/|\Omega_e||\Omega_o| \ll 1$, and then the Rabi frequency is estimated as $|\Omega| \approx \Omega_*(\kappa_o/2|\delta_o|)\sqrt{\mathcal{W}/\mathcal{W}_*}$ [48].

IV. RESULTS

Before using SC conditions to our advantage, we set $|a_\mu\rangle = |b_\mu\rangle e^{-i\beta_\mu t}$ and solve the full dispersion law $\det(\hat{H}_\mu + \hat{V} - \beta_\mu \hat{I}) = 0$ numerically for every μ . Condition $\text{Im}\beta_\mu = 0$ specifies the boundaries between the areas with and without gain. Fig. 1(a) shows the case of $|\Omega|/\kappa_o \gg 1$, and $|\Omega|/\kappa_e \sim 1$, i.e., when we have SC for the ordinary, but not yet for the extraordinary photons. Under these conditions, the μ -specific instability domains are arranged as a sequence of the 4-beam stars shifted along the δ_o , but nearly coinciding along the δ_e , direction. As $|\Omega|$ is increased further and provides $|\Omega|/\kappa_{o,e} \gg 1$,

i.e., $|\Omega| \gg \Omega_*$, we step firmly into the SC regime. Now, a spectacular pattern of the narrow resonances appears along the δ_e direction and the ones along δ_o sharpen even more, see Figs. 1(b),(c).

Thus, the SC condition channels gain into the narrow mode-number specific regions in the parameter space. Parametric frequency conversion in $\chi^{(2)}$ resonators with $\mathcal{F} \sim 10$ - 10^2 , operating in the weak-coupling, i.e., Purcell, regime, that has attracted significant recent attention [52–55], does not have this effect, and the contrast of the star beams in Fig. 1(a) is reduced further for smaller \mathcal{F} . Formation of the narrow instability tongues in the high- \mathcal{F} regime is similar to the Arnold-tongues reported in the high-finesse Kerr microresonators [56, 57]. However, the matrix operator driving the sideband dynamics in Refs. [56, 57] is entirely non-Hermitian, as is \hat{V} here. Therefore, it does not allow to define the energy and momentum for the quasi-particles in the way possible here, if \hat{H}_μ dominates over \hat{V} , i.e., in the SC regime.

To leading order, the mode dynamics in the SC regime is driven by $i\partial_t|a_\mu\rangle = \hat{H}_\mu|a_\mu\rangle$. \hat{H}_μ is block-diagonal and has two orthogonal sub-spaces of the dressed states. The

top-block subspace is span by $|b_\mu^{(1)}\rangle = (|\Omega|e^{-i\phi}, \Delta_\mu - \Omega_\mu, 0, 0)^T$ and $|b_\mu^{(2)}\rangle = (\Omega_\mu - \Delta_\mu, |\Omega|e^{i\phi}, 0, 0)^T$, where

$$\Delta_\mu = \Delta_{\mu o} - \Delta_{\mu e}, \quad (7)$$

is the Rabi detuning, see Eqs. (8). The corresponding eigenfrequencies are $\beta_\mu^{(1)} = \beta_\mu^{(+)}$ and $\beta_\mu^{(2)} = \beta_\mu^{(-)}$,

$$\beta_\mu^{(\pm)} = \frac{1}{2}(\Delta_{\mu o} + \Delta_{\mu e}) \pm \frac{1}{2}\Omega_\mu, \quad \Omega_\mu = \sqrt{\Delta_\mu^2 + |\Omega|^2}. \quad (8)$$

Here, Ω_μ is the effective Rabi frequency [18, 19]. The bottom-block eigenstates and eigenfrequencies are $|b_\mu^{(3)}\rangle = (0, 0, |\Omega|e^{i\phi}, \Delta_{-\mu} - \Omega_{-\mu})^T$, $\beta_\mu^{(3)} = -\beta_{-\mu}^{(+)}$, and $|b_\mu^{(4)}\rangle = (0, 0, \Omega_{-\mu} - \Delta_{-\mu}, |\Omega|e^{-i\phi})^T$, $\beta_\mu^{(4)} = -\beta_{-\mu}^{(-)}$. Each pair of the dressed states makes its own avoided crossing around the momentum values corresponding to $\Delta_{\pm\mu} = 0$, Fig. 2(a). Close to the avoided crossings, the state dressing is increasing via $\Omega_{\pm\mu} - \Delta_{\pm\mu} \rightarrow |\Omega|$.

The frequency-momentum dependencies, $\beta_\mu^{(j)}$ vs μ for $j = 1, 2$ and $j = 3, 4$, Fig. 1(d), define the four families of quasi-particles. These quasi-particles hybridise the $\omega_{\mu o}$ and $\omega_{\mu e}$ photons, and can be naturally called *photon-photon polaritons*. \hat{H}_μ is Hermitian and its eigenfrequencies can be used as the quasi-particle energy spectrum. Hence, the photon-photons carry energy $\varepsilon = \hbar\beta_\mu^{(j)}$ ($\sim \mu\text{eV}$, $D_1 \sim D_{1o}$), angular momentum $\ell = \hbar\mu$, and the linear momentum $k = \ell/R$, where R is the resonator radius. Predictably, there is a flexibility with defining the photon-photon zero-energy level. This is controlled by the reference frame choice, i.e., by D_1 entering $\Delta_{\mu o} + \Delta_{\mu e}$, while Δ_μ and Ω_μ are D_1 independent. The effective photon-photon mass is evaluated as $m_{\text{eff}}^{-1} = \partial_k^2[\hbar\beta_\mu^{(j)}]$. Away from the avoided crossings, the photon-photons behave as photons and have $m_{\text{eff}} \simeq \pm\hbar/R^2|D_{2s}| \sim 10^{-3}m_e$, where m_e is the electron mass. Close to the avoided crossings, SC modifies linear dispersion, and, because of this, m_{eff} can drop by few orders of magnitude, sharply rise to infinity and change its sign, see Fig. 1(e).

Photon-photons make the four spectral families, when their frequencies are recalculated back to the physical spectral range, $\tilde{\omega}_{\mu o}^{(j)} = \omega_p \pm \beta_\mu^{(j)} \pm \mu D_1$ and $\tilde{\omega}_{\mu e}^{(j)} = 2\omega_p \pm \beta_\mu^{(j)} \pm \mu D_1$, where '+' should be used for $j = 1, 2$ and '-' for $j = 3, 4$. While these dressed spectra are not equidistant, they provide equal separation of the sideband lines from the pump and its second harmonic, i.e., $\tilde{\omega}_{\mu o}^{(j)} - \tilde{\omega}_{-\mu o}^{(j)} = \tilde{\omega}_{\mu e}^{(j)} - \tilde{\omega}_{-\mu e}^{(j)}$. This is quite a remarkable observation, since for the bare-photons $((\omega_{\mu o} - \omega_{-\mu o}) - (\omega_{\mu e} - \omega_{-\mu e})) \sim (D_{1o} - D_{1e})|\mu|$ reaches to GHz.

Let us now describe how the dressed spectra allow formulating the TWM and FWM energy conservation laws. TWM drives the Rabi flops between $|\psi_{\mu o}(t)\rangle^2$ and $|\psi_{\mu e}(t)\rangle^2$, and the quanta involved satisfy

$$\hbar\omega_p + \hbar\tilde{\omega}_{\mu o}^{(j)} = \hbar\tilde{\omega}_{\mu e}^{(j)}.$$

The above condition combines a pump photon with a dressed ordinary photon with momentum μ to produce a dressed extraordinary photon with the same μ . The other process, is the cross-branch FWM that engages μ and $-\mu$ quanta and yields the following energy conservation between two pump laser photons and two dressed ordinary polarised quanta,

$$\hbar\omega_p + \hbar\omega_p = \hbar\tilde{\omega}_{\mu o}^{(j_1)} + \hbar\tilde{\omega}_{\mu o}^{(j_2)}, \quad j_1 = 1, 2, \quad j_2 = 3, 4. \quad (9)$$

An important feature of the $\beta_\mu^{(j)}$ vs μ dependencies are the resonances between the photon-photons belonging to the 1, 2 (full circles in Fig. 1(d)) and 3, 4 (empty circles) branches. Four eigenfrequencies generally admit six distinct resonance conditions, $\beta_\mu^{(j_1)} = \beta_\mu^{(j_2)}$. However, all six of them can be realised only for $\Omega = 0$. The dressed resonator, $\Omega \neq 0$, allows for the four resonance conditions $(j_1; j_2) = (1; 3), (1; 4), (2; 3),$ and $(2; 4)$, each yielding the photon energy conservation in Eq. (9). A particular case selected for Fig. 1(d) illustrates two simultaneous resonance conditions $\beta_\mu^{(1)} = \beta_\mu^{(4)}$ and $\beta_\mu^{(2)} = \beta_\mu^{(3)}$. The $(j_1; j_2) = (1; 2)$ and $(3; 4)$ resonances existing for $\Omega = 0$ are replaced with the avoided crossings for $\Omega \neq 0$.

Resolving each of the four resonance conditions for Ω gives the same elegant answer,

$$\frac{|\Omega|^2}{4} = \frac{(\Delta_{\mu o} + \Delta_{-\mu e})(\Delta_{\mu o} + \Delta_{-\mu o})(\Delta_{\mu e} + \Delta_{-\mu e})}{(\Delta_{\mu o} + \Delta_{-\mu o} + \Delta_{\mu e} + \Delta_{-\mu e})^2} \times (\Delta_{\mu e} + \Delta_{-\mu o}). \quad (10)$$

Eq. (10) is structurally similar to the resonant denominators derived for the susceptibilities emerging through the interaction of the multimode fields with the multi-level atoms [16, 18, 19]. The resonance lines computed from Eq. (10) and mapped onto Fig. 1(c) precisely follow the maximal gain lines in the parameter space, i.e., $\max \text{Im}\beta_\mu > 0$ vs δ_s , where the complex β_μ are computed from $\det(\hat{H}_\mu + \hat{V} - \beta_\mu \hat{T}) = 0$. Taking Fig. 1(c), we find that the first and last brackets in Eq. (10) determine the resonance separation along δ_e , which happens in steps $\simeq |D_{1o} - D_{1e}|$, 2nd bracket controls resonances along δ_o in steps of $\simeq |D_{2o}\mu|$, while the 3rd bracket does not make a noticeable impact along δ_e because $|D_{2e}\mu| \ll |D_{1o} - D_{1e}|$.

All resonance lines have a special point triggering a parametric instability relative to the $\pm\mu$ modes. To find the parametric gain threshold when the system is confined to one of the resonances, i.e., when two energy levels are degenerate, $\beta_\mu^{(j_1)} = \beta_\mu^{(j_2)}$, while their eigenvectors remain different, we apply the degenerate state perturbation theory [58] to Eq. (4) by treating the FWM operator \hat{V} as a perturbation. The matrix elements of \hat{V} are $\langle b_\mu^{(j_1)} | \hat{V} | b_\mu^{(j_2)} \rangle = V_\mu^{(j_1 j_2)}$. FWM removes the degeneracy between $\beta_\mu^{(j_1)}$ and $\beta_\mu^{(j_2)}$ by making different the loss vs gain balance acquired by the two states. One state becomes lossy, while the other generates gain providing $V_\mu^{(j_1 j_2)} V_\mu^{(j_2 j_1)} > V_\mu^{(j_1 j_1)} V_\mu^{(j_2 j_2)}$. Opening the above for,

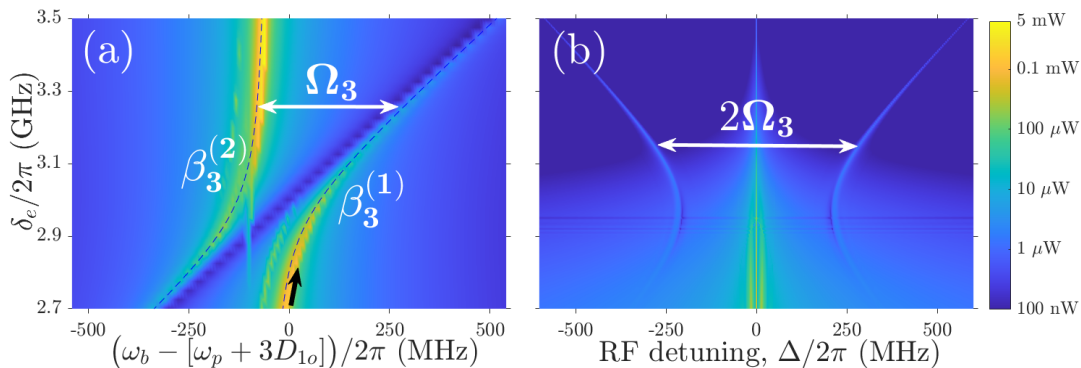


FIG. 2. **(a)** Avoided crossing of the $\beta_3^{(1)}$ and $\beta_3^{(2)}$ photon-photon states as recorded through the series of the numerical scans of the probe frequency, ω_b , for a range of δ_e values. ω_b is scanned around the bare resonator resonance at $\omega_{3o} \simeq \omega_{0o} + 3D_{1o}$. Color density shows the $\mu = 3$ mode power, $\int_0^\tau |\psi_{3o}|^2 dt/\tau$, see color-bar. Parameters are $\mathcal{W}_b = 0.9\text{mW}$ (probe laser power), $\mathcal{W} \simeq 176\text{mW}$ (pump laser power), $\delta_o/2\pi = -50\text{MHz}$, $\tau = 0.4\mu\text{s}$. Corresponding cw-state power, i.e., the one that directly drives nonlinear processes in the resonator material, is $|\tilde{\psi}_o|^2 = \mathcal{H}_*^2 |\Omega|^2 / \Omega_*^2 \simeq (\eta \mathcal{F} \mathcal{W} / 4\pi) \times (\kappa_o / \delta_o)^2 \simeq 60\text{mW}$, which is below \mathcal{W} because the resonator is driven far off-resonance. **(b)** Rabi (Autler-Townes) sidebands in the RF spectrum, $\int_0^\tau |\psi_{3o}|^2 e^{-it\Delta} dt/\tau$ vs δ_e , as computed for the $\beta_3^{(1)}$ polariton branch, see the black arrow in (a). Color-bar applies to both (a) and (b).

e.g., the $(j_1; j_2) = (1; 4)$ case yields

$$\frac{|\Omega|^6}{|\Omega_e|^2} (\Delta_{-\mu} - \Omega_{-\mu})^2 = \frac{1}{4} \times \quad (11)$$

$$(\kappa_o |\Omega|^2 + \kappa_e (\Delta_{-\mu} - \Omega_{-\mu})^2) (\kappa_e |\Omega|^2 + \kappa_o (\Delta_{-\mu} - \Omega_{-\mu})^2).$$

Eq. (11) explicitly expresses the balance between the net gain (left) and the net loss (right). The intersection between the hypersurfaces defined by Eqs. (10) and (11) provides an excellent approximation for the locations of the instability boundary tips, see Fig. 1(c), thereby proving that the resonance effect lies at the origin of the channelling of the parametric gain into narrow instability domains.

Dressing of the spectrum, i.e., splitting of the resonances of the bare, $\Omega = 0$, resonator, and the underpinning Rabi dynamics have been also demonstrated by us in a series of numerical experiments reproducing how the photon-photon realm could be measured in a lab. To achieve this, we consider a region in Fig. 1(c) that avoids the FWM gain, and where the power enhancement effects provided by the resonator are diminished or even reversed, while the SC induced dressing effects on the resonator spectrum can be seen clearly. We then include a weak probe field, 'b', into Eqs. (1), through the transformation $\mathcal{H} \rightarrow \mathcal{H} + \mathcal{H}_b e^{i\mu\vartheta - i(\omega_b - \omega_p)t}$. This probe field has the non-zero projections on the $|b_\mu^{(1)}\rangle$, $|b_\mu^{(2)}\rangle$ dressed states via their ordinary components. Therefore, if ω_b is tuned to the frequency of one of the dressed states, e.g., to $\tilde{\omega}_{\mu o}^{(1)}$, it then resonantly excites a superposition state, $\alpha_1 |b_\mu^{(1)}\rangle e^{-it\beta_\mu^{(1)}} + \alpha_2 |b_\mu^{(2)}\rangle e^{-it\beta_\mu^{(2)}}$, that exhibits Rabi oscillations. These oscillations are expressed as the anti-phase beats of $|\psi_{\mu o}(t)|^2$ and $|\psi_{\mu e}(t)|^2$ with the frequency $\tilde{\omega}_{\mu s}^{(1)} - \tilde{\omega}_{\mu s}^{(2)} = \beta_\mu^{(1)} - \beta_\mu^{(2)} = \Omega_\mu$. The probe laser power, and what it achieves inside the resonator during the frequency scan, is relatively weak, while the pump laser is

kept at the constant frequency far away from the resonance, and therefore they are not expected to cause significant thermal effects, see Fig. 2 for the power and detuning values. Other pump-probe arrangements in Kerr microresonators have been recently demonstrated in Ref. [59]. Further thermal control can be applied with the techniques as the ones developed for cooling of microresonators and photonic chips [60–62].

Fig. 2(a) shows how the $|\psi_{3o}|^2$ power responds to the applied probe depending on its frequency, ω_b , and through a range of the δ_e values. One can see pronounced resonant responses for ω_b tuned to $\tilde{\omega}_{3o}^{(1)}$ and $\tilde{\omega}_{3o}^{(2)}$. This fully confirms our analytical results for the dressed spectrum, see Eqs. (8) and the dashed lines in Fig. 2(a). The avoided crossing region in Fig. 2(a) corresponds to the minimum of Ω_3 in δ_e , i.e., $\Delta_3 = 0$ and $\Omega_3 = |\Omega|$. Same avoided crossings can be observed for the whole sequence of the resonances in the 'star'-diagram in Fig. 1(c). Measurements like in Fig. 2(a) are often used as signatures of the polariton existence in other optical systems, see, e.g., Refs. [4, 21].

Rabi beats can be observed by measuring the RF spectra of either the total field or the individual modes, $\mu = 3$ in this case. Fig. 2(b) shows the spectrum of $|\psi_{3o}(t)|^2$ vs δ_e with ω_b tuned to $\tilde{\omega}_{3o}^{(1)}$. It makes obvious the spectral signature of the Rabi splitting, which is also known as the Autler-Townes splitting in spectroscopy [16, 27, 63]. The sideband power in Fig. 2(b) is proportional to the modulation depth of $|\psi_{3o}(t)|^2$, which is reduced if the probe projection on one of the two dressed states is much larger than on the other, e.g., $|\alpha_1| \gg |\alpha_2|$.

V. SUMMARY

We have proposed and formalised a concept of the polariton quasi-particles, photon-photon polaritons, in the context of multimode high-Q $\chi^{(2)}$ microring resonators. The quasi-particle regime becomes possible if a resonator is pumped far-off the resonance, which allows the dominance of the Hermitian part of the side-band coupling operator over the dissipation and parametric gain effects. Such a resonator operates in the strong-coupling regime, shows the splitting of the resonances, their avoided crossings, and Rabi oscillations between the ordinary and ex-

traordinary modes. Our results reveal a promising connection between the rapidly expanding research area of frequency conversion in high-Q microresonators and the quasiparticle approach widely used in other branches of photonics and condensed matter physics.

ACKNOWLEDGMENTS

This work was supported by the EU Horizon 2020 Framework Programme (812818, MICROCOMB), UK EPSRC (EP/R008159), and Russian Science Foundation (17-12-01413-II).

-
- [1] R. Miller, T.E. Northup, K.M. Birnbaum, A. Boca, A.D. Boozer and H.J. Kimble, Trapped atoms in cavity QED: coupling quantized light and matter, *J. Phys. B: At. Mol. Opt. Phys.* **38**, S551 (2005).
 - [2] H. Kimble, The quantum internet, *Nature* **453**, 1023 (2008).
 - [3] J. Kasprzak, M. Richard, S. Kundermann, A. Baas, P. Jeambrun, J. M. J. Keeling, F. M. Marchetti, M. H. Szymańska, R. André, J. L. Staehli, V. Savona, P. B. Littlewood, B. Deveaud, and L. S. Dang, Bose-Einstein condensation of exciton polaritons, *Nature* **443**, 409 (2006).
 - [4] S. Christopoulos, G. Högersthal, A. J. D. Grundy, P. G. Lagoudakis, A. V. Kavokin, J. J. Baumberg, G. Christmann, R. Butté, E. Feltin, J.-F. Carlin, and N. Grandjean, Room-Temperature Polariton Lasing in Semiconductor Microcavities, *Phys. Rev. Lett.* **98**, 126405 (2007).
 - [5] A. Amo, J. Lefrère, S. Pigeon, C. Adrados, C. Ciuti, I. Carusotto, R. Houdré, E. Giacobino, and A. Bramati, Superfluidity of polaritons in semiconductor microcavities, *Nat. Physics* **5**, 805 (2009).
 - [6] M. Sich, D.N. Krizhanovskii, M.S. Skolnick, A.V. Gorbach, R. Hartley, D.V. Skryabin, E.A. Cerda-Mendez, K. Biermann, R. Hey, and P.V. Santos, Observation of bright polariton solitons in a semiconductor microcavity, *Nat. Photonics* **6**, 50 (2012).
 - [7] L. Dominici, D. Colas, S. Donati, J.P.R. Cuartas, M. De Giorgi, D. Ballarini, G. Guirales, J.C.L. Carreno, A. Bramati, G. Gigli, E. del Valle, F.P. Laussy, and D. Sanvitto, Ultrafast Control and Rabi Oscillations of Polaritons, *Phys. Rev. Lett.* **113**, 226401 (2014).
 - [8] L.B. Tan, O. Cotlet, A. Bergschneider, R. Schmidt, P. Back, Y. Shimazaki, M. Kroner, and A. Imamoglu, Interacting Polaron-Polaritons, *Phys. Rev. X* **10**, 021011 (2020).
 - [9] T.M. Autry, G. Nardin, C.L. Smallwood, K. Silverman, D. Bajoni, A. Lemaître, S. Bouchoule, J. Bloch, and S. Cundiff, Excitation Ladder of Cavity Polaritons, *Phys. Rev. Lett.* **125**, 067403 (2020).
 - [10] Y.V. Kartashov and D.V. Skryabin, Modulational instability and solitary waves in polariton topological insulators, *Optica* **3**, 1228 (2016).
 - [11] L. Yuan, Q. Lin, M. Xiao, and S. Fan, Synthetic dimension in photonics, *Optica* **5**, 1396 (2018).
 - [12] T. Ozawa, H.M. Price, A. Amo, N. Goldman, M. Hafezi, L. Lu, M.C. Rechtsman, D. Schuster, J. Simon, O. Zilberberg, and I. Carusotto, Topological photonics, *Rev. Mod. Phys.* **91**, 015006 (2019).
 - [13] E.T. Jaynes and F.W. Cummings, Comparison of Quantum and Semiclassical Radiation Theory with Application to the Beam Maser, *Proceedings of IEEE* **51**, 89 (1963).
 - [14] Y. Zhu, D. J. Gauthier, S. E. Morin, Q. Wu, H. J. Carmichael, and T. W. Mossberg, Vacuum Rabi splitting as a feature of linear-dispersion theory: Analysis and experimental observations, *Phys. Rev. Lett.* **64**, 2499 (1990).
 - [15] M. Brune, F. Schmidt-Kaler, A. Maali, J. Dreyer, E. Hagley, J. M. Raimond, and S. Haroche, Quantum Rabi Oscillation: A Direct Test of Field Quantization in a Cavity, *Phys. Rev. Lett.* **76**, 1800 (1996).
 - [16] C. Cohen-Tannoudji and S. Reynaud, Dressed-atom description of resonance fluorescence and absorption spectra of a multi-level atom in an intense laser beam, *J. Phys. B: At. Mol. Opt. Phys.* **10**, 345 (1977).
 - [17] D. D. Yavuz, A. V. Sokolov, and S. E. Harris, Eigenvectors of a Raman Medium, *Phys. Rev. Lett.* **84**, 75 (1999).
 - [18] M.O. Scully and M.S. Zubairy, *Quantum Optics* (Cambridge University Press, 2006).
 - [19] R. Boyd, *Nonlinear optics* (Academic Press, 2008).
 - [20] L. Landau, Theory of the Superfluidity of Helium II, *Phys. Rev.* **60**, 356 (1941).
 - [21] P. Torma and W.L. Barnes, Strong coupling between surface plasmon polaritons and emitters: a review, *Rep. Prog. Phys.* **78**, 013901 (2015).
 - [22] T.K. Hakala, A.J. Moilanen, A.I. Vakevainen, R. Guo, J.P. Martikainen, K.S. Daskalakis, H.T. Rekola, A. Julku, and P. Torma, Bose-Einstein condensation in a plasmonic lattice, *Nat. Physics* **14**, 739 (2018).
 - [23] D.E. Chang, V. Vuletic, and M.D. Lukin, Quantum nonlinear optics - photon by photon, *Nat. Photonics* **8**, 685 (2014).
 - [24] A.L. Gaeta, M. Lipson, and T.J. Kippenberg, Photonic-chip-based frequency combs, *Nat. Photonics* **13**, 158 (2019).
 - [25] M. Kues, C. Reimer, J.M. Lukens, W.J. Munro, A.M. Weiner, D.J. Moss, and R. Morandotti, Quantum optical microcombs, *Nat. Photonics* **13**, 170-179 (2019).
 - [26] T. Aoki, B. Dayan, E. Wilcut, W.P. Bowen, A.S. Parkins, T.J. Kippenberg, K.J. Vahala, and H. J. Kimble, Observation of strong coupling between one atom and a mono-

- lithic microresonator, *Nature* **443**, 671–674 (2006).
- [27] B. Peng, S. K. Ozdemir, W. Chen, F. Nori, and L. Yang, What is and what is not electromagnetically induced transparency in whispering-gallery microcavities, *Nat. Commun.* **5**, 5082 (2014).
- [28] S. Ramelow, A. Farsi, Z. Vernon, S. Clemmen, X. Ji, J.E. Sipe, M. Liscidini, M. Lipson, and A. L. Gaeta, Strong Nonlinear Coupling in a Si_3N_4 Ring Resonator, *Phys. Rev. Lett.* **122**, 153906 (2019).
- [29] Y. Sherkunov, D.M. Whittaker, and V. Fal’ko, Rabi oscillations of two-photon states in nonlinear optical resonators, *Phys. Rev. A* **93**, 023843 (2016).
- [30] Z. Vernon, M. Liscidini, and J.E. Sipe, Quantum frequency conversion and strong coupling of photonic modes using four-wave mixing in integrated microresonators, *Phys. Rev. A* **94**, 023810 (2016).
- [31] S. Schiller and R. L. Byer, Quadruply resonant optical parametric oscillation in a monolithic total-internal-reflection resonator, *J. Opt. Soc. Am. B* **10**, 1696-1707 (1993).
- [32] V. Berger, Second-harmonic generation in monolithic cavities, *J. Opt. Soc. Am. B* **14**, 1351-1360 (1997).
- [33] A.V. Buryak, P. Di Trapani, D.V. Skryabin, and S. Trillo, Optical solitons due to quadratic nonlinearities: from basic physics to futuristic applications, *Phys. Rep.* **370**, 63 (2002).
- [34] V.S. Ilchenko, A.A. Savchenkov, A.B. Matsko, and L. Maleki, Nonlinear Optics and Crystalline Whispering Gallery Mode Cavities, *Phys. Rev. Lett.* **92**, 043903 (2004).
- [35] J.U. Fürst, D.V. Strelakov, D. Elser, M. Lassen, U. L. Andersen, C. Marquardt, and G. Leuchs, Naturally phase-matched second harmonic generation in a whispering-gallery-mode resonator, *Phys. Rev. Lett.* **104**, 153901 (2010).
- [36] J. U. Fürst, D. V. Strelakov, D. Elser, A. Aiello, U. L. Andersen, Ch. Marquardt, and G. Leuchs, Low-Threshold Optical Parametric Oscillations in a Whispering Gallery Mode Resonator, *Phys. Rev. Lett.* **105**, 263904 (2010).
- [37] T. Beckmann, H. Linnenbank, H. Steigerwald, B. Sturman, D. Haertle, K. Buse, and I. Breunig, Highly Tunable Low-Threshold Optical Parametric Oscillation in Radially Poled Whispering Gallery Resonators, *Phys. Rev. Lett.* **106**, 143903 (2011).
- [38] I. Carusotto and G. C. La Rocca, Two-photon Rabi splitting and optical Stark effect in semiconductor microcavities, *Phys. Rev. B* **60**, 4907 (1999).
- [39] M. Zhang, C. Wang, R. Cheng, A. Shams-Ansari, and M. Loncar, Monolithic ultra-high-Q lithium niobate microring resonator, *Optica* **4**, 1536 (2017).
- [40] Y. He, Q.-F. Yang, J. Ling, R. Luo, H. Liang, M. Li, B. Shen, H. Wang, K. Vahala, and Q. Lin, A self-starting bi-chromatic LiNbO_3 soliton microcomb, *Optica* **6**, 1138 (2019).
- [41] I. Hendry, L.S. Trainor, Y. Xu, S. Coen, S.G. Murdoch, H.G. Schwefel, and M. Erkintalo, Experimental observation of internally pumped parametric oscillation and quadratic comb generation in a chi((2)) whispering-gallery-mode microresonator, *Opt. Lett.* **45**, 1204 (2020).
- [42] A.W. Bruch, X. Liu, J.B. Surya, C.-L. Zou, and H.X. Tang, On-chip $\chi^{(2)}$ microring optical parametric oscillator, *Optica* **6**, 1361 (2019).
- [43] A.W. Bruch, X. Liu, Z. Gong, J.B. Surya, M. Li, C.L. Zou, and H. Tang, Pockels Soliton Microcomb, *Nat. Photonics* **15**, 21 (2021).
- [44] J. Szabados, D.N. Puzyrev, Y. Minet, L. Reis, K. Buse, A. Villois, D.V. Skryabin, and I. Breunig, Frequency comb generation via cascaded second-order nonlinearities in microresonators, *Phys. Rev. Lett.* **124**, 203902 (2020).
- [45] O.A. Egorov and D.V. Skryabin, Frequency comb generation in a resonantly pumped exciton-polariton microring resonator, *Opt. Express* **26**, 24003 (2018).
- [46] T.S. Haugland, E. Ronca, E.F. Kjonstad, A. Rubio, and H. Koch, Coupled Cluster Theory for Molecular Polaritons: Changing Ground and Excited States, *Phys. Rev. X* **10**, 041043 (2020).
- [47] D.V. Skryabin, Coupled-mode theory for microresonators with quadratic nonlinearity, *J. Opt. Soc. Am B* **37**, 2604 (2020).
- [48] See Supplemental Material at [URL will be inserted by publisher] for more details on parameter values.
- [49] H. Suchowski, D. Oron, A. Arie, and Y. Silberberg, Geometrical representation of sum frequency generation and adiabatic frequency conversion, *Phys. Rev. A* **78**, 063821 (2008).
- [50] A. Karnieli, and A. Arie, Fully controllable adiabatic geometric phase in nonlinear optics, *Opt. Express* **26**, 4920 (2018).
- [51] R. Schiek, H. Fang, R. Malendevich, and G.I. Stegeman, Measurement of Modulational Instability Gain of Second-Order Nonlinear Optical Eigenmodes in a One-Dimensional System, *Phys. Rev. Lett.* **86**, 4528 (2001).
- [52] J. Roslund, R. de Araujo, S. Jiang, C. Fabre, and N. Treps, Wavelength-multiplexed quantum networks with ultrafast frequency combs, *Nat. Photonics* **8**, 109 (2014).
- [53] V. Ulvila, C.R. Phillips, L. Halonen, and M. Vainio, High-power mid-infrared frequency comb from a continuous-wave-pumped bulk optical parametric oscillator, *Opt. Express* **22**, 10535 (2014).
- [54] F. Leo, T. Hansson, I. Ricciardi, M. De Rosa, S. Coen, S. Wabnitz, and M. Erkintalo, Walk-Off-Induced Modulation Instability, Temporal Pattern Formation, and Frequency Comb Generation in Cavity-Enhanced Second-Harmonic Generation, *Phys. Rev. Lett.* **116**, 033901 (2016).
- [55] S. Mosca, M. Parisi, I. Ricciardi, F. Leo, T. Hansson, M. Erkintalo, P. Maddaloni, P. De Natale, S. Wabnitz, and M. De Rosa, Modulation Instability Induced Frequency Comb Generation in a Continuously Pumped Optical Parametric Oscillator, *Phys. Rev. Lett.* **121**, 093903 (2018).
- [56] D.V. Skryabin, Z. Fan, A. Villois, and D.N. Puzyrev, Threshold of complexity and Arnold tongues in Kerr ring microresonators, *Phys. Rev. A* **103**, L011502 (2021).
- [57] D.N. Puzyrev and D.V. Skryabin, Finesse and four-wave mixing in microresonators, *Phys. Rev. A* **103**, 013508 (2021).
- [58] E. Fermi, *Notes on Quantum Mechanics* (University of Chicago Press, 1995).
- [59] G.N. Ghalanos, J.M. Silver, L. Del Bino, N. Moroney, S. Zhang, M.T.M. Woodley, A. Svela, and P. Del’Haye, Kerr-Nonlinearity-Induced Mode-Splitting in Optical Microresonators, *Phys. Rev. Lett.* **124**, 223901 (2020).
- [60] G. Moille, X. Lu, A. Rao, Q. Li, D.A. Westly, L. Ranzani, S.B. Papp, M. Soltani, and K. Srinivasan, Kerr-

- Microresonator Soliton Frequency Combs at Cryogenic Temperatures, *Phys. Rev. Applied* **12**, 034057 (2019).
- [61] T.E. Drake, J.R. Stone, T.C. Briles, and S.B. Papp, Thermal decoherence and laser cooling of Kerr microresonator solitons, *Nat. Photonics* **14**, 480 (2020).
- [62] G.F. Sinclair, N.A. Tyler, D. Sahin, J. Barreto, and M.G. Thompson, Temperature Dependence of the Kerr Nonlinearity and Two-Photon Absorption in a Silicon Waveguide at $1.55\mu\text{m}$, *Phys. Rev. Applied* **11**, 044084 (2019).
- [63] M.F. Limonov, M.V. Rybin, A.N. Poddubny, and Y.S. Kivshar, Fano resonances in photonics, *Nat. Photonics* **11** 543 (2017).